Analytical and Bioanalytical Chemistry https://doi.org/10.1007/s00216-023-04690-y

RESEARCH PAPER

Scanning ion conductance microscopy reveals differential effect of $PM_{2.5}$ exposure on A549 lung epithelial and SH-SY5Y neuroblastoma cell membranes

Christina Dhoj[1] · Adaly Garcia[1] · Artur Manasyan[1] · Miriam Benavides[1] · Dana Abou Abbas[2] · Cindy Toscano[2] · Edith Porter[2] · Yixian Wang[1]

Received: 29 December 2022 / Revised: 13 March 2023 / Accepted: 3 April 2023

Abstract

Numerous studies have linked a wide range of diseases including respiratory illnesses to harmful particulate matter (PM) emissions indoors and outdoors, such as incense PM and industrial PM. Because of their ability to penetrate the lower respiratory tract and the circulatory system, fine particles with diameters of 2.5 μm or less ($PM_{2.5}$) are believed to be more hazardous than larger PMs. Despite the enormous number of studies focusing on the intracellular processes associated with $PM_{2.5}$ exposure, there have been limited reports studying the biophysical properties of cell membranes, such as nanoscale morphological changes induced by $PM_{2.5}$. Our study assesses the membrane topographical and structural effects of $PM_{2.5}$ from incense $PM_{2.5}$ exposure in real time on A549 lung carcinoma epithelial cells and SH-SY5Y neuroblastoma cells that had been fixed to preclude adaptive cell responses. The size distribution and mechanical properties of the $PM_{2.5}$ sample were characterized with atomic force microscopy (AFM). Nanoscale morphological monitoring of the cell membranes utilizing scanning ion conductance microscopy (SICM) indicated statistically significant increasing membrane roughness at A549 cells at half an hour of exposure and visible damage at 4 h of exposure. In contrast, no significant increase in roughness was observed on SH-SY5Y cells after half an hour of $PM_{2.5}$ exposure, although continued exposure to $PM_{2.5}$ for up to 4 h affected an expansion of lesions already present before exposure commenced. These findings suggest that A549 cell membranes are more susceptible to structural damage by $PM_{2.5}$ compared to SH-SY5Y cell membranes, corroborating more enhanced susceptibility of airway epithelial cells to exposure to $PM_{2.5}$ than neuronal cells. **Keywords** SICM · Particulate matter · Membrane topography · Single-cell imaging

Introduction

With growing population density, vehicular usage, and corporate emissions, among many other sources of pollution, particulate matter (PM) has exponentially grown into a significant concern for the health and safety of the global population, especially in heavily polluted urban cities such as Los Angeles, CA, USA [1–3]. PM pollution is also associated with indoor activities such as incense stick burning, cooking, cigarette smoking, fireplace utilization, and ventilation systems [4–6]. Fine particles with diameters of 2.5 μm or less are specified as P $M_{2.5}$, which are believed to be more hazardous than larger PMs because of the ability of P $M_{2.5}$ to penetrate the circulatory system and the lower respiratory tract, increasing respiratory and cardiovascular diseases [7–10]. $PM_{2.5}$ can increase free radical production (e.g., hydroxyl radical, •OH) in human cells, consume antioxidant ingredients, and cause oxidative stress [11]. $PM_{2.5}$-induced oxidative stress plays a key role in autophagy in lung cells and may contribute to the impairment of pulmonary function [12]. Elevated production of •OH can

Published online: 18 April 2023

Published in the topical collection *Young Investigators in (Bio-) Analytical Chemistry 2023* with guest editors Zhi-Yuan Gu, Beatriz Jurado-Sánchez, Thomas H. Linz, Leandro Wang Hantao, Nongnoot Wongkaew, and Peng Wu.

✉ Yixian Wang
ywang184@calstatela.edu

[1] Department of Chemistry and Biochemistry, California State University, Los Angeles, Los Angeles, CA 90032, USA

[2] Department of Biological Sciences, California State University, Los Angeles, Los Angeles, CA 90032, USA

cause oxidative damage to DNA, further inducing teratogenesis, carcinogenesis,

mutagenesis, and other irreversible damages [7, 13]. Other hypothesized mechanisms for the damaging effects of P $M_{2.5}$ include imbalanced intracellular calcium homeostasis and inflammatory injury [7], and reduction of the mitochondrial dehydrogenase activity [14]. Long-term $PM_{2.5}$ exposure was also associated with increased risks of neurological disorders such as dementia, Alzheimer's disease, and Parkinson's disease [15–19]. There are multiple possible pathways for PM $_{2.5}$ to damage the integrity of the blood-brain barrier and penetrate the brain and cause harm [20, 21]. Intracellular effects of harmful P $M_{2.5}$, such as decreased ATP levels, increased C a^{2+} levels, oxidative stress, inflammation, and an increase of mitochondrial function as exposure time increases, have been reported for neuronal systems [22–25].

Despite the enormous number of studies focusing on the intracellular processes associated with P $M_{2.5}$ exposure, there have been limited reports on studying the biophysical properties of cell membranes, such as nanoscale morphological changes, that are associated with P $M_{2.5}$. Expanding on how particulate matter affects cellular membrane structure can provide new insight into the mechanism of P $M_{2.5}$-induced cell damage and add valuable information to the intersection of health consequences and the environmental particulate matter issue. In addition, most reported works focused on biological processes that occurred upon long-term exposure (> 24 h) to $PM_{2.5}$. Being able to monitor the effect during the initial stage of exposure (up to 4 h) would also be important to understand how the damage is initiated.

Here we report on the effect of short-term P $M_{2.5}$ exposure on human cell membranes at the nanoscale using scanning ion conductance microscopy (SICM). SICM is a topographical imaging technique that utilizes the ionic current that flows between an electrode inside a nanopipette and a second electrode that resides in the bulk solution as a surfacesensitive feedback signal to map the sample's topography [26–28]. Importantly, SICM can image the cell membrane topographies with nanometer precision without using chemical probes and is not likely to damage or distort biological samples throughout imaging since it exerts a negligible force on the sample [29, 30]. From the SICM images, membrane roughness, defined as the root-mean-square deviation of *z*-heights across the membrane surface, can be extracted and used to evaluate the membrane topographical changes [31, 32]. Two cell lines, the lung-derived cell line A549 and the neuroblastoma-derived cell line SH-SY5Y, were chosen as models to mimic the toxic effect of $PM_{2.5}$ on human cells and compare the effect on different cell lines. The former are adenocarcinoma human alveolar type II–like epithelial cells, commonly used as models for the study of lung diseases [33, 34], and have been extensively applied to study $PM_{2.5}$-induced cell toxicities [12, 35–38]. SH-SY5Y cells are commonly used to mimic neuronal cells for the studies of neurological disorders [39, 40] and have been used for studying $PM_{2.5}$ exposure–induced cytotoxicity, mitochondrial dysfunction and oxidative stress, and apoptosis [22, 23, 41]. Both A549 and SH-SY5Y cells were exposed to $PM_{2.5}$ collected from incense stick burning, and the morphological changes were monitored with SICM and compared. Cells had been fixed before P $M_{2.5}$ exposure to prolong the imaging time, preclude different cell adaptive responses or quick cell death–induced topographical changes, and highlight the physical changes of the cell membranes [31, 42, 43]. Fixation itself has been proven not to significantly affect the membrane topography in SICM images [29].

Experimental

Chemicals and materials

Phosphate-buffered saline (PBS) tablets (Thermo Fisher Scientific, Waltham, MA); PBS 1X solution (Corning, Durham, NC); formaldehyde solution (37.0%, SigmaAldrich, St. Louis, MO); 4% paraformaldehyde (Santa Cruz Biotechnology, Inc, Dallas, TX); F12-K medium supplemented with 2 mM L-glutamine and 1500 mg/L sodium bicarbonate (ATCC, Manassas, VA); Dulbecco's modified Eagle medium (DMEM) with Ham's F-12 nutrient mixture, L-glutamine, and HEPES (Corning, Durham, NC); fetal bovine serum (heat inactivated, Corning, Durham, NC); and penicillin-streptomycin (Research Product International, Mount Prospect, IL) were used without further purification. All solutions were prepared from double-deionized water (resistivity = 18.2 MΩ*cm at 25 °C, Milli-Q Ultrapure water EQ 7000 Purification System, MilliporeSigma, Burlington, MA). Unless stated otherwise, disposable materials were purchased from Thermo Fisher Scientific. PBS solutions prepared from tablets were filtered through a 0.02-µm pore size syringe filter (Thermo Fisher Scientific, Waltham, MA).

A549 cell culture

The A549 cell line was obtained from ATCC. Cells were thawed according to the manufacturer's instructions, seeded in 35-mm Petri dishes (about 1 × 10^6 cells per dish), and

incubated in F-12 K medium containing 2 mM L-glutamine, 1500 mg/L sodium bicarbonate, and 10% FBS at 37 °C and 5% CO_2 until 40% confluency was reached. Before SICM imaging and $PM_{2.5}$ exposure, to preclude adaptive cell responses, the cells were fixed for 10 min at room temperature using 3.7% formaldehyde (diluted from 37% stock solution with PBS), washed briefly with PBS, and then submerged in 3 mL of filtered PBS.

SH-SY5Y cell culture

SH-SY5Y neuroblastoma cells were obtained from ATCC and grown under standard culture conditions (37 °C and 5% carbon dioxide) in Dulbecco's modified Eagle medium with Ham's F-12 nutrient mixture, L-glutamine, and HEPES supplemented with fetal bovine serum (10% v/v) and penicillin-streptomycin (1%). Trypsin (0.25%) was used to detach cells from culture plates for sample splitting. Cells were then cultured in 35-mm Petri dishes until 40% confluency was reached. Prior to SICM imaging and $PM_{2.5}$ exposure, to preclude adaptive cell responses, the cells were fixed for 10 min using 4% paraformaldehyde at room temperature, washed briefly with PBS, and then submerged in 3 mL of filtered PBS.

$PM_{2.5}$ exposure

Collection of $PM_{2.5}$ was adapted from similar collection methods [4–6]. $PM_{2.5}$ samples for cell exposure tests were collected from burning a Kayuragi incense stick (Nippon Kodo, Inc., Torrance, CA.). Specifically, the burning smoke from a stick was collected by a 50-mL conical tube for 15 min, followed by adding 10 mL of filtered PBS solution and sonicating for 15 min. P $M_{2.5}$ was always freshly collected for each test. Prior to exposure, SICM images were collected at individual fixed cells. For $PM_{2.5}$ exposure, the PBS solution in the petri dish of fixed cells was carefully removed and replaced with the same volume of the $PM_{2.5}$ solution. The cells were exposed to $PM_{2.5}$ for 30 min prior to P $M_{2.5}$ removal and the addition of fresh, filtered PBS before imaging post-exposure. For the exposure experiments of up to 4 h, continuous SICM imaging was conducted without removing the P $M_{2.5}$ solution. For negative control tests, the PBS solution in the petri dish was removed and restored with the same volume of the same PBS solution.

SICM

Nanopipette SICM probes were pulled from quartz capillaries (1.0 mm outer diameter, 0.50 mm inner diameter, 7.5 cm length, Sutter Instruments, Novato, CA) using a P-2000 laser-based micropipette puller (Sutter Instruments). A typical pulling program is heat = 780, filament = 4, velocity = 15, delay = 120, and pull = 115, which have been confirmed to produce nanopipettes with a radius of 70–100 nm [44]. The nanopipettes were filled with filtered PBS and fitted with Ag/AgCl electrodes. All images were acquired with a Park NX12 multifunctional microscopy platform (Park Systems) equipped with a detachable SICM head, mounted on a Nikon Ti-U inverted optical microscope (Nikon Inc.), and operated with SmartScan (Park Systems). A CCD camera (Pike F-032B, Allied Vision, Exton, PA) was connected to the optical microscope to assist in probe positioning.

Fixed cells in PBS were brought into focus to choose a single cell for imaging. The pipette probe was immersed in the PBS solution, and a potential bias was applied between the pipette and bath electrodes to give an electrolytic current of 1 nA. After the probe was positioned above a target cell, it was approached incrementally with a set point of 98% of the baseline current. Images were acquired in approach-retractscan (ARS) mode. Unless otherwise stated, all images were acquired at the pixel resolution of 128 × 128. SICM images were processed with XEI (Suwon, South Korea). For every pair of before and after exposure scans at the same location, the membrane roughness was measured as the root-meansquare deviation of z-heights across the membrane surface in five cropped sections of 1–3 μm size while avoiding membrane structures. All values were extracted after flattening the cropped sections with regression order 2 using XEI. A two-sample t test with unequal variance (Microsoft Excel 15.0, Microsoft Corporation, Redmond, WA) was then performed to determine the significance of roughness changes.

Results and discussion

SICM monitoring of the effect from 30-min $PM_{2.5}$ exposure

Prior to exposure, the size distribution and mechanical properties of the $PM_{2.5}$ sample, collected either by

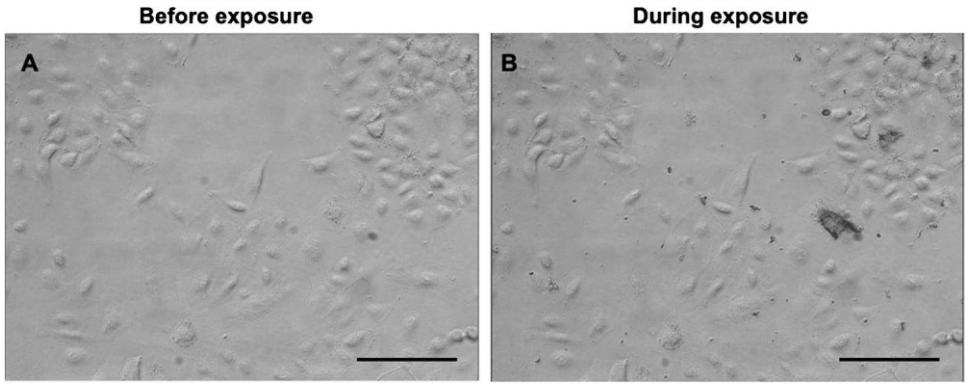

Fig. 1 Representative brightfield images of A549 cells before (**A**) and during (**B**) $PM_{2.5}$ exposure. The scale bar is representative of 100 μm

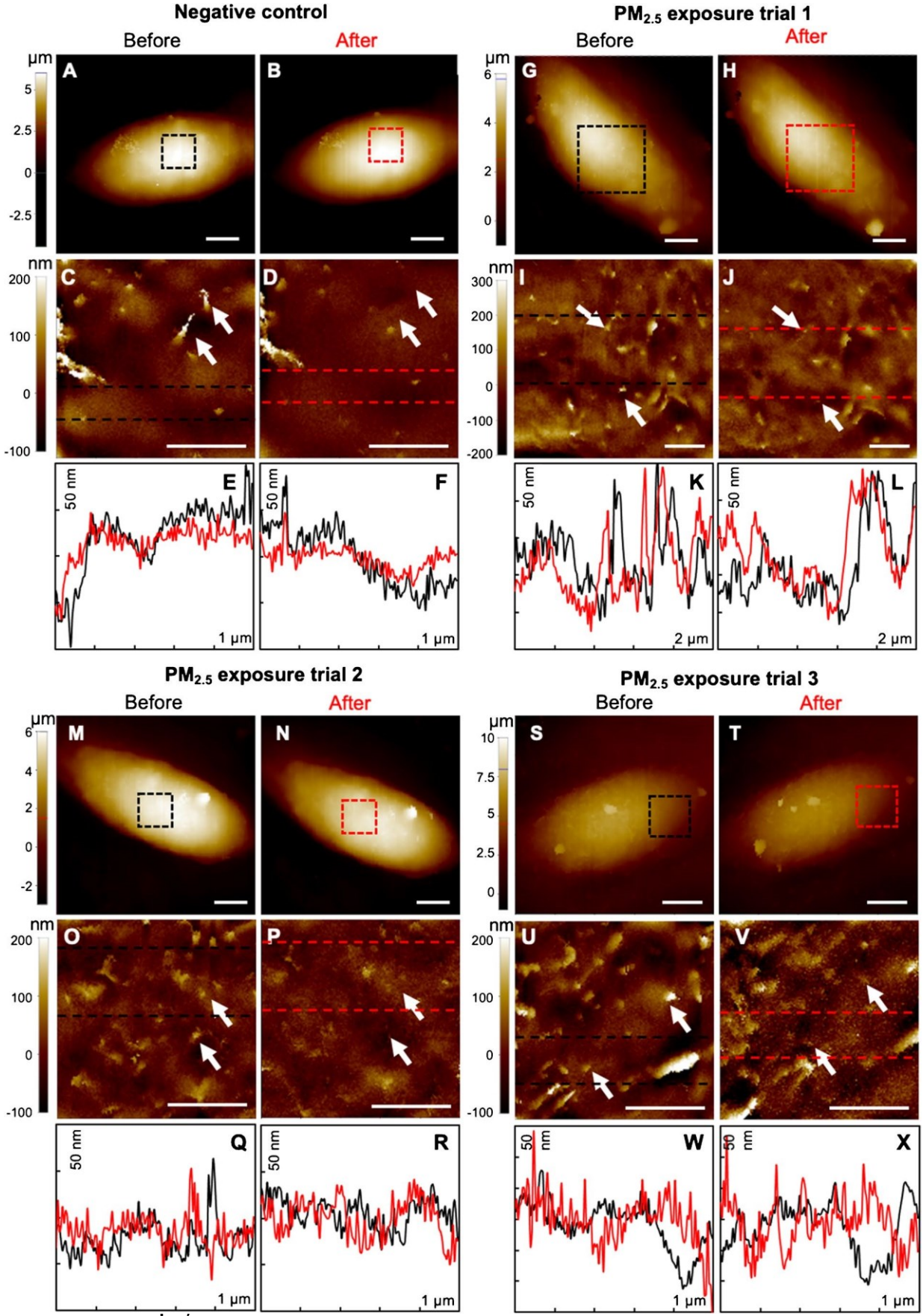
Negative control
Before
After
PM2.5 exposure trial 1
Before
After
PM2.5 exposure trial 2
Before
After
PM2.5 exposure trial 3
Before
After
µm
nm
50 nm
1 µm
2 µm

Fig. 2 Representative SICM images and height profiles of A549 epithelial lung cells. **A**–**D** Control trial images of an A549 cell before (**A**, **C**) and after replacing the solution with PBS and subsequent incubation for 30 min (**B**, **D**). **G**–**J**, **M**–**P**, **S**–**V** Images from three independent experimental trials of P $M_{2.5}$ exposure before (**G**, **H**; **M**, **N**; **S**, **T**) and after (**I**, **J**; **O**, **P**; **U**, **V**) 30 min of $PM_{2.5}$ exposure. Within each trial, the top two are whole-cell images with the scale bar of 5 µm, while the bottom two are zoom-in scans of the areas labeled by the dashed boxes with the scale bar of 2 µm. Whole-cell images were not processed, while the zoom-ins were second-order flattened using XEI to better present the surface features. **E**, **F**; **K**, **L**; **Q**, **R**; **W**, **X** Height profiles extracted from the zoom-in SICM images (C, D; I, J; O, P; U, V) either before (black) or after (red) treatment, with the location labeled by the dashed lines in the corresponding images. In each trial, the left set of height profiles refer to the top dashed line while the right to the bottom dashed line. White arrows point to examples of membrane protrusions that diminished after exposure

directly adhering to a flat mica substrate during burning or depositing to a petri dish in solution to mimic the cell exposure condition, were characterized with atomic force microscopy (AFM). The experimental details and the results and discussion can be found in the supporting information. Briefly, AFM topography characterization (Fig. S1) has demonstrated that the sample meets $PM_{2.5}$ standards with > 90% particles being under 2.5 µm. The adhesion force (Fig. S2) from 14 different particles shows a mean ± 95% CI of (− 14.7 ± 4.9) nN, which is similar to − 25 nN reported by Shi et al. [45]. Such a high adhesiveness is believed to increase the retaining of toxic chemicals and might play a key role in the delivery of pollutants to human cells [45].

Figure 1 shows an example of A549 cell exposure to $PM_{2.5}$ monitored under a bright-field microscope (10×). Before exposure, the area under observation was clear of particles (Fig. 1A), while after replacing the medium with a $PM_{2.5}$ solution, particles of various sizes appeared. The majority of the particles are around or under micrometers in size, as expected by AFM, although a few very large particles (tens of micrometers) were also present, which were not caught by the AFM characterization likely due to the limitation of scanning size. We have avoided imaging cells that are impacted by these oversized particles.

The membrane morphological changes due to exposure to $PM_{2.5}$ at both A549 epithelial cells and SH-SY5Y cells were monitored with SICM. We conducted one control trial and three independent experimental trials for each cell line. In each trial, a single cell was selected and scanned for a full image, from which two to three sub-cell locations were scanned to provide information at a higher resolution. Representative SICM images from A549 epithelial cells are shown in Fig. 2. A549 cells are often used as models of alveolar type II pulmonary epithelial cells enriched with membrane protrusions [46, 47], which increase the surface area of the cell exposed to the lumen and reflect ongoing secretion into the lumen [48]. As shown in Fig. 2, all trials, including the control, showed that the protrusions on the cell surface (see white arrows pointing at examples) diminished after the treatment with either PBS or $PM_{2.5}$, suggesting that the protrusions are very sensitive to the movement of the surrounding solution regardless of the solution composition. However, a roughness increase across the cell membrane, excluding the protrusions, was only observed in the $PM_{2.5}$-exposed trials but not in the control trials. It was most apparent in trial 3 when comparing Fig. 2 U and V, where V obviously has more roughness. Height profiles were extracted to present a more direct comparison of the membranes. The peak-to-peak roughness of the height profiles in trial 3 obviously increased from ~ 20 nm (Fig. 2W, black) before to > 50 nm (Fig. 2W, red) after exposure.

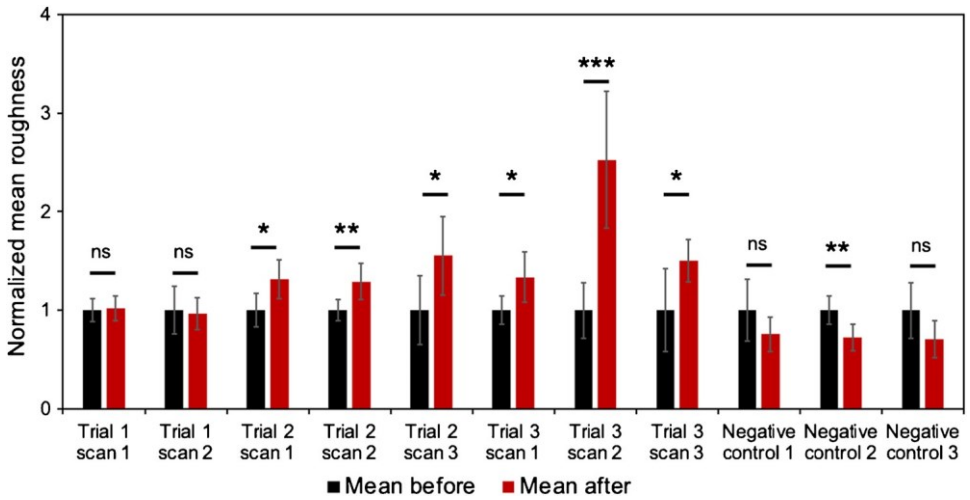

Fig. 3 Statistical comparisons of the mean roughness values before and after treatment for all scans on A549 cells. Data are the mean ± SD, $n = 5$; ns = not significant, *$p < 0.05$, **$p < 0.01$, and ***$p < 0.001$. All trials were normalized by the mean roughness of the corresponding before-exposure data

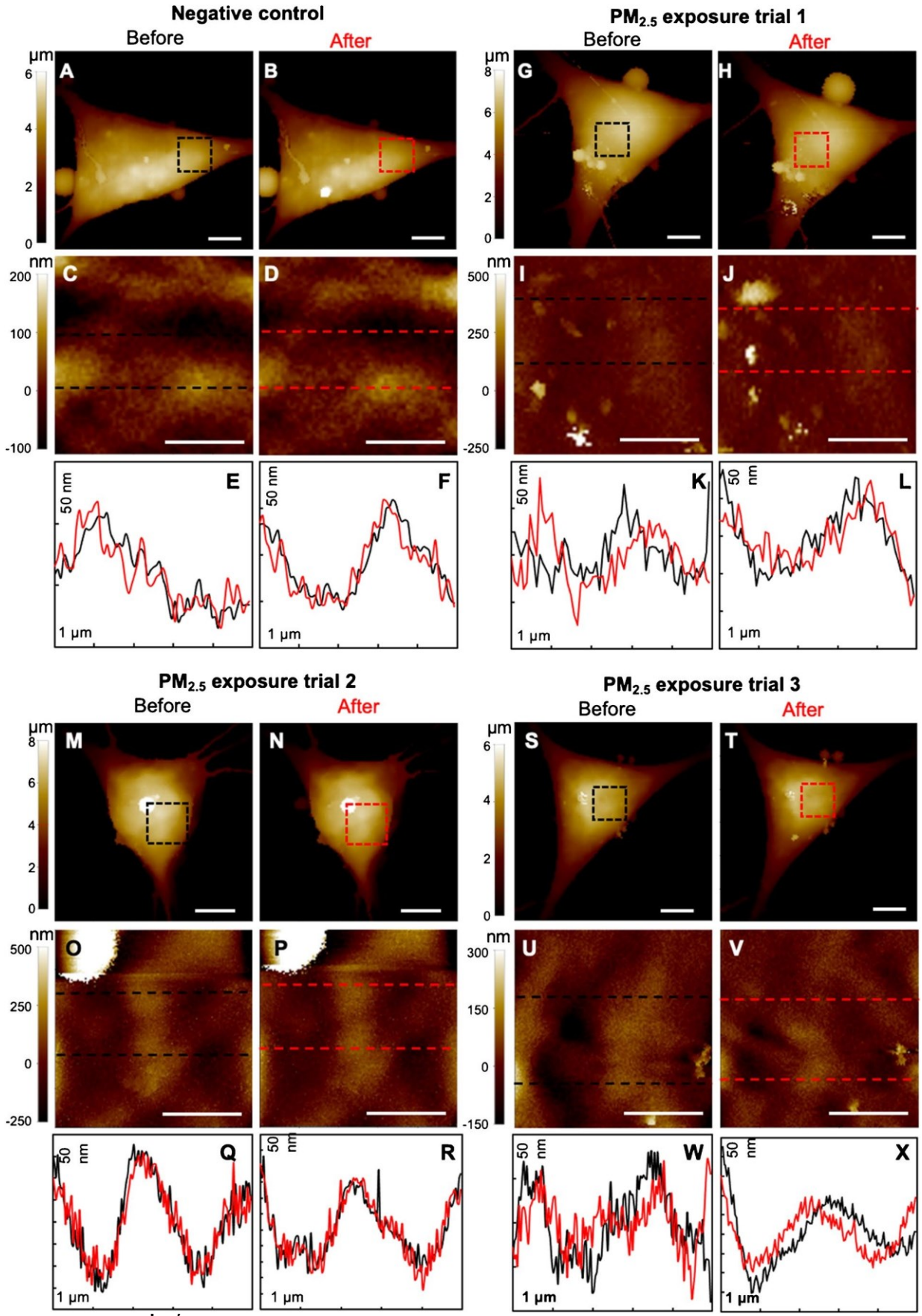
Negative control
Before
After
PM2.5 exposure trial 1
Before
After
PM2.5 exposure trial 2
Before
After
PM2.5 exposure trial 3
Before
After
µm
nm
50 nm
1 µm
A
B
C
D
E
F
G
H
I
J
K
L
M
N
O
P
Q
R
S
T
U
V
W
X

◂ **Fig. 4** Representative SICM images of SH-SY5Y cells. **A**–**D** Control trial images of an SH-SY5Y cell before (**A**, **C**) and after replacing the solution with PBS and subsequent incubation for 30 min (**B**, **D**). **G**–**J**, **M**–**P**, **S**–**V** Images from three independent experimental trials of $PM_{2.5}$ exposure before (**G**, **H**; **M**, **N**; **S**, **T**) and after (**I**, **J**; **O**, **P**; **U**, **V**) 30 min of P $M_{2.5}$ exposure. Within each trial, the top two are whole-cell images with the scale bar of 5 µm, while the bottom two are zoom-in scans of the areas labeled by the dashed boxes with the scale bar of 2 µm. Whole-cell images were not processed, while the zoom-ins were second-order flattened using XEI to better present the surface features. **E**, **F**; **K**, **L**; **Q**, **R**; **W**, **X** Height profiles extracted from the zoom-in SICM images on top of them either before (black) or after (red) treatment, with the location labeled by the dashed lines in the corresponding images. In each trial, the left set of height profiles refer to the top dashed line while the right to the bottom dashed line

We further quantified the mean membrane roughness of every pair of images obtained before and after exposure and statistically compared them. The detailed description of this part of data analysis can be found in the supporting information with Fig. S3. The roughness values before and after treatment were then statistically compared using a *t* test. Figure 3 shows the roughness comparison for all A549 trials. Six out of the eight total scans from three independent A549 exposure trials showed a statistically significant increase in roughness, while none of the control scans did. Note that each trial contained multiple scans of different locations on a single cell; thus, the discrepancy in roughness analysis among trials (trials 1 vs. trials 2 and 3) can be attributed to the cell of interest in each trial interacting with different amounts of particles in solution. This also highlights the capability of revealing the sample heterogeneity by conducting single-cell analysis. As for the control, only the second scan showed a significant change, but it was a decrease in roughness instead of an increase. An increase in membrane roughness can indicate the particles adhering to the surface of the membrane [35], which could subsequently trigger several changes in live cells. Socha-Chafre et al. have shown that PM exposure promotes upregulation of the expression of adhesion molecules, causing an increase in cellular adhesion of particles in vitro [38]. As adhesion occurs on the membrane, particles can inhibit substance exchange and signal transmission into cells, thus causing dysfunction to occur [38]. Moreover, the roughness of the cell membrane could indicate the cell's health state [49].

In contrast to A549 cells, SH-SY5Y cells (Fig. 4) are mostly free of protrusions, consistent with topographical observations from other studies [32, 44, 50]. In general, the morphological alteration was much less visible than in A549 cells, as reflected by both the images and height profiles. The height profiles in trials 2 and 3 have more data points than those in the negative control and trial 1 due to the different pixel numbers present in the images, but this should not affect our conclusion since each comparison was made within a trial, and the scans within each trial always used the same parameters. For the quantitative analysis of roughness, only one of the seven scans showed a statistical increase in roughness after exposure to P $M_{2.5}$ across all three trials (Fig. 5), suggesting different physical properties of the SH-SY5Y cell membrane compared to the A549 cell membrane. This observation suggests that A549 cells are possibly more susceptible to short-term $PM_{2.5}$ damage than SH-SY5Y cells.

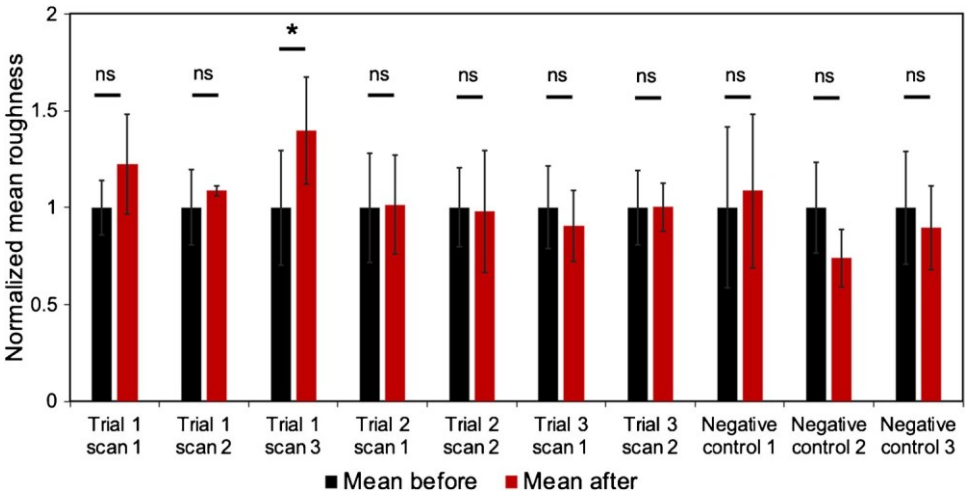

Fig. 5 Statistical comparisons of the mean roughness values before (black) and after (red) treatment for all scans on SH-SY5Y cells. Data are the mean ± SD, $n = 5$; ns = not significant, $*p < 0.05$

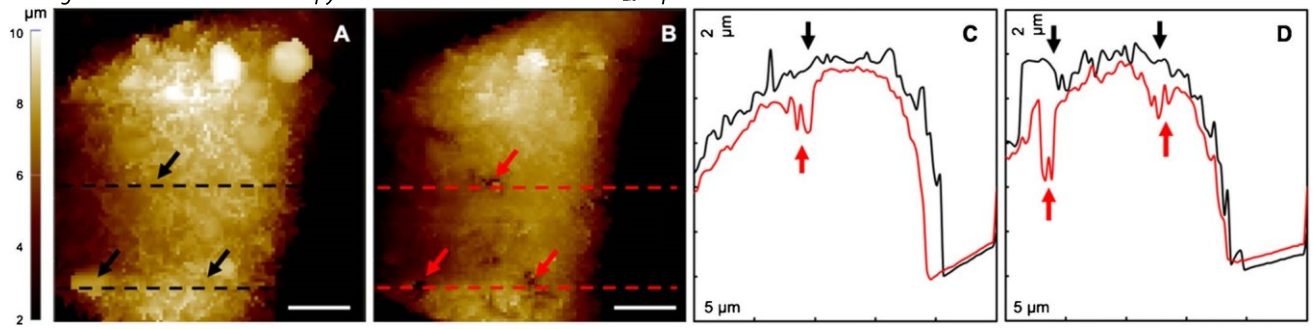

Fig. 6 SICM images of a portion of an A549 epithelial lung cell before (**A**) and after (**B**) continuous exposure to P $M_{2.5}$ solution for 4 h. The scale bar is representative of 5 μm. **C** and **D** are height profiles extracted from the dashed lines in **A** and **B**. **C** was extracted from the top dashed line from before (black) and after (red) exposure to $PM_{2.5}$ solution, while D was extracted from the bottom dashed line. The black (**A**) and red (**B**) arrows point to the same locations before (black) and after (red) exposure, with the red arrows highlighting the membrane disturbances in height profiles that were not observed at the locations pointed at by the black arrows (**C** and **D**)

SICM monitoring of the effect of up to 4 h of $PM_{2.5}$ exposure

We also investigated longer exposure (up to 4 h) to test whether a time-dependent effect exists. A pair of images from the same A549 cell before (Fig. 6A) and after exposure for 4 h (Fig. 6B) shows indentations of 2–4μm depth (Fig. 6C and D, labeled with red arrows) that could reflect pore formation. Specifically, large surface structures, possibly reflecting lamellar bodies (Fig. 6A, black arrows in the bottom), detached from the membrane after P $M_{2.5}$ exposure, leaving indentations on the membrane (Fig. 6B, red arrows). Although fixed cells were used in this study, and thus biological processes cannot be claimed during exposure to P $M_{2.5}$, the morphological evidence found in this study shows that the adhesion of particles caused the disintegration of lamellar bodies and mechanical damages. This observation provides further evidence that P $M_{2.5}$ causes damage to cell membrane integrity in A549 cells, which was previously reported by Liu et al. using the LDH assay that quantifies LDH release to cell media upon damage to the plasma membrane as a measure of the cytotoxic effect of the treatment [51]. To demonstrate that the damage was caused by P $M_{2.5}$ exposure rather than prolonged soaking, possible movement of the solution, or continuous SICM scanning, we carried our negative control tests using PBS as the exposure solution. As shown in Fig. S4, there was no alteration as observed with the experimental trials. We also have previously demonstrated prolonged SICM scanning does not alter the cell membrane through continuously scanning along the same line [52].

The longer exposure test with SH-SY5Y cells exhibited differences in membrane disturbances compared to A549 cells (Fig. 7). Post-exposure damage was found to only occur at the locations where pre-existing defects were present on the dendrite branch. The defects deepened over time, as labeled by red arrows in Fig. 7. A portion of the top of the cell seems to dissipate at 248 min of exposure (Fig. 7D). Representative height profiles extracted from two separate locations, one at a dendrite (Fig. 7E) and the other at a preexisting defect area (Fig. 7F), also indicate a gradual building up of damages to the membrane structures. No damage was observed for other areas that exhibit a smooth surface and fewer structures on the membrane. We also carried negative control tests (Fig. S5) and demonstrated that prolonged soaking and scanning did not alter the membrane structure of the cells to the degree observed in the experimental trial. This suggests that $PM_{2.5}$ effects are more disruptive with cells that exhibit pre-existing defects in the membrane allowing for particles to adhere in defective, open areas reflecting further membrane degradation over time.

Conclusion

Particulate matter is an environmental pollutant with a demonstrated potential for toxicity. To better understand the mechanism of $PM_{2.5}$-induced physical damage to human cells, we investigated the changes in membrane topography of fixed A549 lung carcinoma epithelial cells and SH-SY5Y neuroblastoma cells upon exposure to incense stick–generated particulate matter using SICM. Short-term exposure of 30 min resulted in an immediate, statistically significant increase in membrane roughness for most A549 cells. SHSY5Y cells with smoother membrane surfaces, on the other hand, experienced minimal and mostly non-significant changes in membrane roughness after exposure. Longer exposure of up to 4 h resulted in detached structures consistent with lamellar bodies on the membrane surface of A549 cells, leaving indentations in the membrane, while for SHSY5Y cells, only cells with pre-existing defects exhibited increasing alterations at the site of the pre-existing lesions, but not where the cell membrane has a smooth surface.

Our study focused purely on the mechanical and physical interaction between P $M_{2.5}$ and cell membranes by using fixed cells that excluded any cellular responses. The different observations between A549 and SH-SY5Y cells

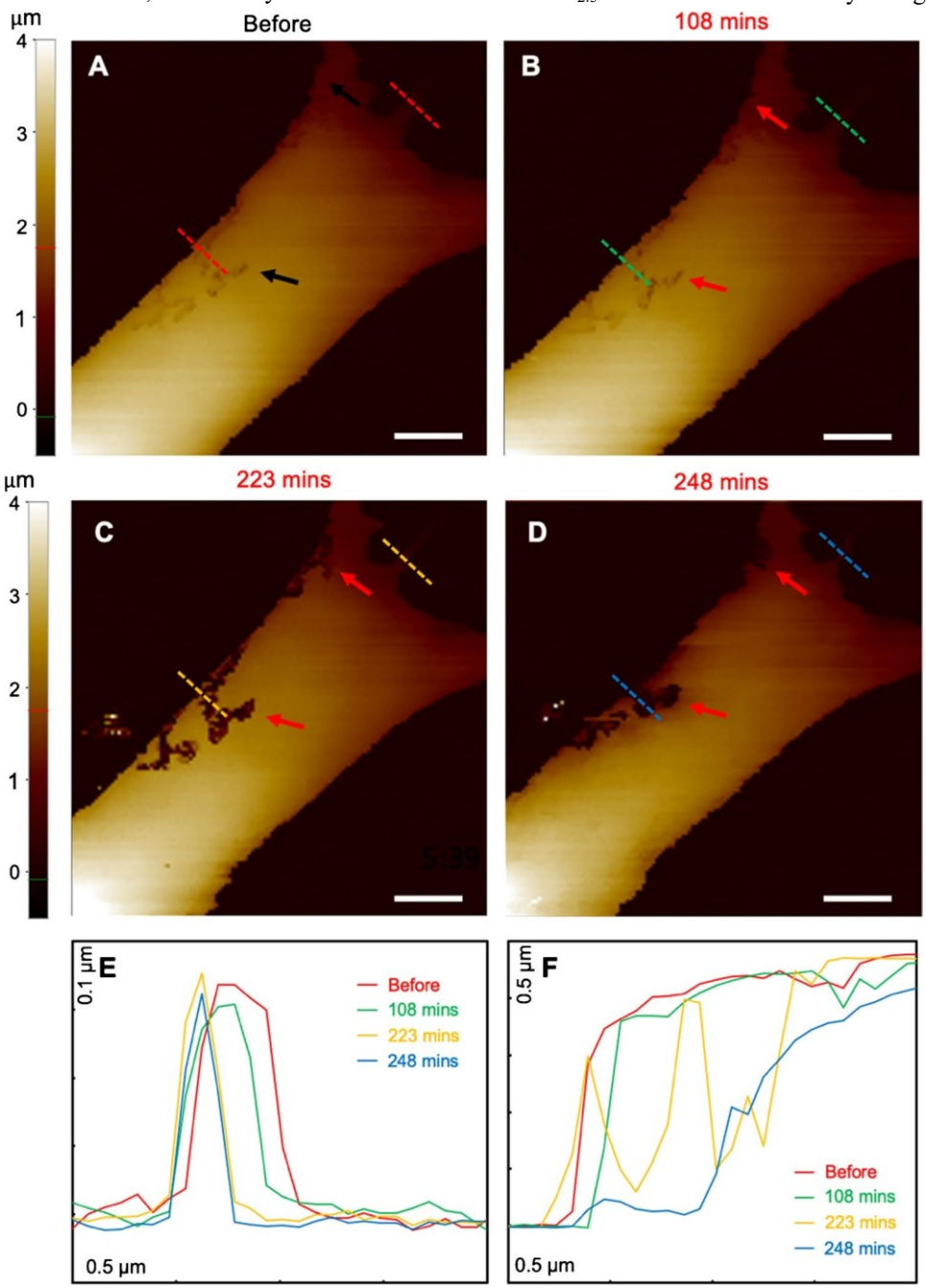

Fig. 7 SICM images of SHSY5Y cells before (**A**) and after (**B**–**D**) over-time exposure to $PM_{2.5}$ solution. The scale bar is representative of 2 µm. The time labels in **B**–**D** represent the exposure time. Height profiles (**E**, **F**) were extracted from the right top corner dashed lines (**E**) and left dashed lines (**F**). Black arrows point to pre-existing defects on the SH-SY5Y cells before $PM_{2.5}$ exposure, and red arrows point to the defects after continuous $PM_{2.5}$ exposure

indicate that the lung cells appear to be generally more susceptible to $PM_{2.5}$ damage, likely due to the fast absorption of the particles that adhere to the surface membrane microstructures. Dissecting the physical properties of $PM_{2.5}$ and cell interaction may aid in understanding the biological potency of $PM_{2.5}$ as a toxic pollutant.

Supplementary Information The online version contains supplementary material available at https://d oi.org/1 0 .1007 /s 00216-023-0 4690- y.

Acknowledgements This work was supported by NIH R15 NS120157 for YW. AG acknowledges the financial support from NSF CHE 2045839. MB acknowledges the financial support from NSF PREM DMR-1523588. CT and EP acknowledge the financial support from NIH R25 GM061331, and DA and EP acknowledge support from the 2022 CSUPERB Faculty Graduate Student Collaboration Award. The authors appreciate the facility support from NSF HRD-1547723.

Declarations

Conflict of interest The authors declare no competing interests.

References

1. Zhang R, Wang G, Guo S, Zamora ML, Ying Q, Lin Y, Wang W, Hu M, Wang Y. Formation of urban fine particulate matter. Chem Rev. 2015;115:3803–55. https:// doi. org/ 10. 1021/ acs. chemr ev. 5b000 67.
2. Karagulian F, Belis CA, Dora CFC, Prüss-Ustün AM, Bonjour S, Adair-Rohani H, Amann M. Contributions to cities' ambient particulate matter (PM): a systematic review of local source contributions at global level. Atmos Environ. 2015;120:475–83. https:// doi. org/ 10. 1016/j. atmos env. 2015. 08.0 87.
3. Ali MU, Liu G, Yousaf B, Ullah H, Abbas Q, Munir MAM. A systematic review on global pollution status of particulate matter-associated potential toxic elements and health perspectives in urban environment. Environ Geochem Health. 2019;41:1131– 62. https:// doi. org/ 10. 1007/ s10653- 018- 0203-z.
4. Li Z, Wen Q, Zhang R. Sources, health effects and control strategies of indoor fine particulate matter (PM2.5): a review. Sci Total Environ. 2017;586:610–622. https:// doi. org/ 10. 1016/j. scito tenv. 2017. 02. 029.
5. Lowther SD, Jones KC, Wang X, Whyatt JD, Wild O, Booker D. Particulate matter measurement indoors: a review of metrics, sensors, needs, and applications. Environ Sci Technol. 2019;53:11644–56. https:// doi. org/ 10. 1021/ acs. est. 9b034 25.
6. Glytsos T, Ondráček J, Džumbová L, Kopanakis I, Lazaridis M. Characterization of particulate matter concentrations during controlled indoor activities. Atmos Environ. 2010;44:1539–49. https:// doi. org/ 10. 1016/j. atmos env. 2010.0 1. 009.
7. Xing YF, Xu YH, Shi MH, Lian YX. The impact of PM2.5 on the human respiratory system. J Thorac Dis. 2016;8:E69–E74. https:// doi. org/ 10. 3978/j. issn. 2072- 1439.2 016. 01. 19.
8. Weichenthal SA, Godri Pollitt K, Villeneuve PJ. PM2.5, oxidant defence and cardiorespiratory health: a review. Environ Heal. 2013;12:40. https:// doi. org/ 10. 1186/ 1476- 069X- 12- 40.
9. Hamanaka RB, Mutlu GM. Particulate matter air pollution: effects on the cardiovascular system. Front Endocrinol (Lausanne). 2018;9:1–15. https://d oi.org/1 0 .3389 /f endo.2018.0 068 0.
10. Brook RD, Rajagopalan S, Pope CA, et al. Particulate matter air pollution and cardiovascular disease. Circulation. 2010;121:2331– 78. https:// doi. org/ 10. 1161/ CIR. 0b013 e3181 dbece1.
11. Donaldson K. Free radical activity associated with the surface of particles: a unifying factor in determining biological activity? Toxicol Lett. 1996;88:293–8. https:// doi. org/ 10. 1016/ 0378-4274(96) 03752-6.
12. Deng X, Zhang F, Rui W, Long F, Wang L, Feng Z, Chen D, Ding W. PM2.5-induced oxidative stress triggers autophagy in human lung epithelial A549 cells. Toxicol Vitr. 2013;27:1762–1770. https:// doi. org/ 10. 1016/j. tiv. 2013. 05. 004.
13. Mehta M, Chen L-C, Gordon T, Rom W, Tang M. Particulate matter inhibits DNA repair and enhances mutagenesis. Mutat Res Toxicol Environ Mutagen. 2008;657:116–21. https:// doi. org/ 10. 1016/j. mrgen tox. 2008. 08. 015.
14. Ferraz ERA, Rainho CR, Fernandes AS, Felzenszwalb I. Differential toxicity of an organic PM 2.5 extract to human lung cells cultured in three dimensions (3D) and monolayers. J Toxicol Environ Heal Part A. 2016;79:221–231. https://d oi.org/1 0 .1080/1 528 7 394. 2016. 11439 02.
15. Rhew SH, Kravchenko J, Lyerly HK. Exposure to low-dose ambient fine particulate matter PM2.5 and Alzheimer's disease, nonAlzheimer's dementia, and Parkinson's disease in North Carolina. PLoS ONE. 2021;16:e0253253. https:// doi. org/ 10. 1371/ journ al. pone. 02532 53.
16 . Fu P, Guo X, Cheung FMH, Yung KKL. The association between PM2.5 exposure and neurological disorders: a systematic review and meta-analysis. Sci Total Environ. 2019;655:1240–1248. https:// doi. org/ 10. 1016/j. scito tenv. 2018. 11. 218.
17. Shi L, Wu X, Danesh Yazdi M, et al. Long-term effects of PM2·5 on neurological disorders in the American Medicare population: a longitudinal cohort study. Lancet Planet Heal. 2020;4:e557–65. https:// doi. org/ 10. 1016/ S2542- 5196(20) 30227-8.
18. Yuan X, Yang Y, Liu C, et al. Fine particulate matter triggers α-synuclein fibrillization and Parkinson-like neurodegeneration. Mov Disord. 2022;37:1817–30. https://d oi.org/1 0 .1002 /m ds.2918 1.
19. Block ML, Calderón-Garcidueñas L. Air pollution: mechanisms of neuroinflammation and CNS disease. Trends Neurosci. 2009;32:506–16. https:// doi. org/ 10. 1016/j. tins. 2009. 05. 009.
20 . Shou Y, Huang Y, Zhu X, Liu C, Hu Y, Wang H. A review of the possible associations between ambient PM2.5 exposures and the development of Alzheimer's disease. Ecotoxicol Environ Saf. 2019;174:344–352. https://d oi.org/1 0 .1016 /j.e coenv.2019.0 2 .086 .
21. Xiong Q, Tian X, Xu C, Ma B, Liu W, Sun B, Ru Q, Shu X. PM2.5 exposure-induced ferroptosis in neuronal cells via inhibiting ERK/ CREB pathway. Environ Toxicol. 2022;37:2201–2213. https://d oi. org/ 10. 1002/ tox. 23586.
22. Wang Y, Zhang M, Li Z, Yue J, Xu M, Zhang Y, Yung KKL, Li R. Fine particulate matter induces mitochondrial dysfunction and oxidative stress in human SH-SY5Y cells. Chemosphere. 2019;218:577–88. https:// doi. org/ 10. 1016/j. chemo sphere. 2018. 11. 149.
23. Zhang M, Wang Y, Wong RMS, Yung KKL, Li R. Fine particulate matter induces endoplasmic reticulum stress-mediated apoptosis in human SH-SY5Y cells. Neurotoxicology. 2022;88:187–95. https:// doi. org/ 10. 1016/j. neuro. 2021. 11. 012.

24. Lin C-H, Nicol CJB, Wan C, Chen S-J, Huang R-N, Chiang M-C. Exposure to PM2.5 induces neurotoxicity, mitochondrial dysfunction, oxidative stress and inflammation in human SH-SY5Y neuronal cells. Neurotoxicology. 2022;88:25–35. https:// doi. org/ 10. 1016/j. neuro. 2021. 10. 009.
25. Li Z, Tian F, Ban H, Xia S, Cheng L, Ren X, Lyu Y, Zheng J. Energy metabolism disorders and oxidative stress in the SHSY5Y cells following PM2.5 air pollution exposure. Toxicol Lett. 2022;369:25–33. https:// doi. org/ 10. 1016/j. toxlet. 2022. 08. 008.
26 . Korchev YE, Bashford CL, Milovanovic M, Vodyanoy I, Lab MJ. Scanning ion conductance microscopy of living cells. Biophys J. 1997;73:653–8. https://d oi.org/1 0 .1016 /S 0006-3495(97)7 8100- 1.
27. Chen C-C, Zhou Y, Baker L a. Scanning ion conductance microscopy. Annu Rev Anal Chem. 2012;5:207–228. https://d oi.org/1 0 . 1146/ annur ev- anchem- 062011- 143203.
28 . Zhu C, Huang K, Siepser NP, Baker LA. Scanning ion conductance microscopy. Chem Rev. 2021;121:11726–68. https://d oi.org/ 10. 1021/ acs. chemr ev. 0c009 62.
29. Seifert J, Rheinlaender J, Novak P, Korchev YE, Schäffer TE. Comparison of atomic force microscopy and scanning ion conductance microscopy for live cell imaging. Langmuir. 2015;31:6807–13. https://d oi.org/1 0 .1021 /a cs.langmu ir .5 b0112 4.
30. Happel P, Thatenhorst D, Dietzel I. Scanning ion conductance microscopy for studying biological samples. Sensors. 2012;12:14983–5008. https:// doi. org/ 10. 3390/ s1211 14983.
31. Rubfiaro AS, Tsegay PS, Lai Y, Cabello E, Shaver M, Hutcheson J, Liu Y, He J. Scanning ion conductance microscopy study reveals the disruption of the integrity of the human cell membrane structure by oxidative DNA damage. ACS Appl Bio Mater. 2021;4:1632–9. https:// doi. org/ 10. 1021/ acsabm. 0c0146 1.
32. Parres-Gold J, Chieng A, Wong SuS, Wang Y. Real-time characterization of cell membrane disruption by α-synuclein oligomers in live SH-SY5Y neuroblastoma cells. ACS Chem Neurosci. 2020;11:2528–34. https://d oi.org/1 0 .1021 /a cschemneur o .0 c0030 9.
33. Giard DJ, Aaronson SA, Todaro GJ, Arnstein P, Kersey JH, Dosik H, Parks WP. In vitro cultivation of human tumors: establishment of cell lines derived from a series of solid tumors2. JNCI J Natl Cancer Inst. 1973;51:1417–23. https:// doi. org/ 10. 1093/ jnci/ 51.5. 1417.
34. Carterson AJ, Höner zu Bentrup K, Ott CM, Clarke MS, Pierson DL, Vanderburg CR, Buchanan KL, Nickerson CA, Schurr MJ. A549 Lung epithelial cells grown as three-dimensional aggregates: alternative tissue culture model for pseudomonas aeruginosa pathogenesis. Infect Immun. 2005;73:1129–1140. https:// doi. org/ 10. 1128/ IAI. 73.2. 1129- 1140. 2005.
35. Gualtieri M, Mantecca P, Corvaja V, Longhin E, Perrone MG, Bolzacchini E, Camatini M. Winter fine particulate matter from Milan induces morphological and functional alterations in human pulmonary epithelial cells (A549). Toxicol Lett. 2009;188:52–62. https:// doi. org/ 10. 1016/j. toxlet. 2009. 03. 003.
36. Tang M, Wang Y, Tang D, Xiu P, Yang Z, Chen Y, Wang H. Influence of the PM 2.5 water-soluble compound on the biophysical properties of A549 cells. Langmuir. 2021;37:4042–4048. https:// doi. org/ 10. 1021/ acs. langm uir. 1c005 22.
37. Chen Y, Luo XS, Zhao Z, Chen Q, Wu D, Sun X, Wu L, Jin L. Summer–winter differences of PM2.5 toxicity to human alveolar epithelial cells (A549) and the roles of transition metals. Ecotoxicol Environ Saf. 2018;165:505–509. https://d oi.org/1 0 .1016 /j. ecoenv. 2018. 09. 034.
38. Soca-Chafre G, Avila-Vásquez H, Rueda-Romero C, Huerta-García E, Márquez-Ramírez SG, Ramos-Godinez P, López-Marure R, Alfaro-Moreno E, Montiel-Dávalos A. Airborne particulate matter upregulates expression of early and late adhesion molecules and their receptors in a lung adenocarcinoma cell line. Environ Res. 2021;198:111242. https:// doi. org/ 10. 1016/j. envres. 2021. 111242.
39. Fusco G, Chen SW, Williamson PTF, et al. Structural basis of membrane disruption and cellular toxicity by α-synuclein oligomers. Science (80-). 2017;358:1440–1443. https:// doi. org/ 10. 1126/ scien ce. aan61 60.
40. Xicoy H, Wieringa B, Martens GJM. The SH-SY5Y cell line in Parkinson's disease research: a systematic review. Mol Neurodegener. 2017;12:10. https://d oi.org/1 0 .1186 /s 13024-017-0 149- 0.
41. Ferraro SA, Astort F, Yakisich JS, Tasat DR. Particulate matter cytotoxicity in cultured SH-SY5Y cells is modulated by simvastatin: toxicological assessment for oxidative damage. Neurotoxicology. 2016;53:108–14. https://d oi.org/1 0 .1016 /j.n euro.2016.0 1 .00 3.
42. Hagemann P, Gesper A, Happel P. Correlative stimulated emission depletion and scanning ion conductance microscopy. ACS Nano. 2018;12:5807–15. https:// doi. org/ 10. 1021/ acsna no. 8b017 31.
43. Nakajima M, Mizutani Y, Iwata F, Ushiki T. Scanning ion conductance microscopy for visualizing the three-dimensional surface topography of cells and tissues. Semin Cell Dev Biol. 2018;73:125–31. https://d oi.org/1 0 .1016 /j.s emcdb.2017.0 9 .02 4.
44. Feng C, Flores M, Dhoj C, Garcia A, Belleca S, Abbas DA, Parres-Gold J, Anguiano A, Porter E, Wang Y. Observation of α-synuclein preformed fibrils interacting with SH-SY5Y neuroblastoma cell membranes using scanning ion conductance microscopy. ACS Chem Neurosci. 2022;13:3547–53. https:// doi. org/ 10. 1021/ acsch emneu ro. 2c004 78.
45. Shi Y, Ji Y, Sun H, et al. Nanoscale characterization of PM2.5 airborne pollutants reveals high adhesiveness and aggregation capability of soot particles. Sci Rep. 2015;5:11232. https://d oi. org/ 10. 1038/ srep1 1232.
46. Jiang R, Shen H, Piao Y-J. The morphometrical analysis on the ultrastructure of A549 cells. Rom J Morphol Embryol. 2010;51:663–7.
47. Fehrenbach H, Schmiedl A, Wahlers T, Hirt SW, Brasch F, Riemann D, Richter J. Morphometric characterisation of the fine structure of human type II pneumocytes. Anat Rec. 1995;243:49–62. https:// doi. org/ 10. 1002/ ar. 10924 30107.
48. Fischer RS. Move your microvilli. J Cell Biol. 2014;207:9–11. https:// doi. org/ 10. 1083/ jcb. 20140 9059.
49 . Antonio PD, Lasalvia M, Perna G, Capozzi V. Scale-independent roughness value of cell membranes studied by means of AFM technique. Biochim Biophys Acta Biomembr. 2012;1818:3141–3148. https:// doi. org/ 10. 1016/j. bbamem. 2012. 08. 001.
50. Fang Y, Iu CYY, Lui CNP, Zou Y, Fung CKM, Li HW, Xi N, Yung KKL, Lai KWC. Investigating dynamic structural and mechanical changes of neuroblastoma cells associated with glutamate-mediated neurodegeneration. Sci Rep. 2015;4:7074. https:// doi. org/ 10. 1038/ srep0 7074.
51 . Liu L, Zhou Q, Yang X, Li G, Zhang J, Zhou X, Jiang W. Cytotoxicity of the soluble and insoluble fractions of atmospheric fine particulate matter. J Environ Sci. 2020;91:105–16. https://d oi.org/ 10. 1016/j. jes. 2020. 01. 012.

52. Wong SuS, Chieng A, Parres-Gold J, Chang M, Wang Y. Realtime determination of aggregated alpha-synuclein induced membrane disruption at neuroblastoma cells using scanning ion conductance microscopy. Faraday Discuss. 2018;210:131–43. https:// doi. org/ 10. 1039/ C8FD0 0059J.